Poly(amidoamine)s carrying TEMPO residues for NMR imaging applications

Maristella Gussoni,*[a] Fulvia Greco,[b] Paolo Ferruti,[c] Elisabetta Ranucci,[c] Alessandro Ponti[d] and Lucia Zetta*[b]

Received (in Montpellier, France) 21st August 2007, Accepted 20th September 2007
First published as an Advance Article on the web 8th October 2007
DOI: 10.1039/b712896g

An amphoteric bio-compatible and stealth-like poly (amidoamine) named ISA23 was obtained from 2,2-bis(acrylamido)acetic acid (BAC) and 2-methylpiperazine. The partial substitution of 4-amino-2,2,6,6-tetramethylpiperidin-1-oxyl (Amino-TEMPO) for 2-methylpiperazine as co-monomer gave two new PAA-TEMPO conjugates based on ISA23: ISA23-TEMPO1 and ISA23-TEMPO2 with 10 and 40% TEMPO-carrying units per polymer chain, respectively. In this study, a thorough NMR characterization of ISA23 polymer together with NMR and ESR characterizations of the ISA23-TEMPO derivatives and a preliminary evaluation of their potential as NMR labels for imaging applications are reported. Relaxivity measurements performed on ISA23-TEMPO1 and ISA23-TEMPO2 showed relaxivities of 0.4 and 1.8 mM^{-1} s^{-1}, respectively, indicating that the PAA-TEMPO adducts have a definite potential as NMR imaging contrast agents. This was confirmed by preliminary magnetic resonance imaging (MRI) determinations.

1 Introduction

Magnetic resonance imaging (MRI) is a commonly used clinical imaging procedure that provides images of soft tissue anatomy with excellent detail. This method has been largely used for non-invasive diagnosis and characterization of tumors and related pathological conditions, as well as for devising appropriate cancer treatment approaches.

A great deal of research on this topic has been focused on the use of paramagnetic inorganic ion chelates, such as gadolinium derivatives, which received the greatest clinical utilization as contrast agents. However, stable free radicals, including nitroxides, may prove useful as MRI contrast agents.

Nitroxyl radicals can be easily conjugated to various (bio)-molecules and particles, owing to their chemical flexibility, easy preparation and excellent stability at physiological pH and temperature. They show limited *in vivo* metabolism, do not cross the blood-brain barrier and undergo glomerular filtration† as a dominant route of elimination. In particular, 2,2,6,6-tetramethylpiperidin-1-oxyl (TEMPO) exhibits increased relaxation rate as do paramagnetic ions attached to macromolecules. The stability of this nitroxyl radical can be attributed in part to the steric hindrance provided by the four methyl groups and in part to the delocalization of the unpaired electron away from oxygen and toward the nitrogen atom. In fact, many nitroxyl radicals may undergo chemical transformations in other sectors of the molecule without affecting the free radical moiety.

A large number of publications have appeared in the literature involving nitroxyl radicals as living polymerization agents, magnetic materials, therapeutic agents, radical scavengers, contrast agents and drugs, just to mention a few.[1–5] Indeed, they have been used as spin labelling agents for electron spin resonance (ESR) spectroscopy and contrast agents for magnetic resonance imaging (MRI).[6–9] Very recently, nitroxyl radicals have been widely used as spin probes for low-frequency *in vivo* ESR imaging, as contrast agents for Overhauser imaging.[10]

Owing to their paramagnetic nature and thus their ability to affect the relaxation times T_1 and T_2 of nearby nuclei, nitroxide free radicals represent a class of potential MRI contrast-enhancing agents which are not toxic at low dosages.[7,8]

Reasonable pharmacokinetic features, such as that the imaging agent reaches its intended target at sufficient concentration and remains there for sufficient time to be detectable in living tissues, are mandatory for the externally administered nitroxyl agents. Nevertheless, obstacles such as premature metabolic conversion of nitroxides to their non-paramagnetic state, rapid excretion, non specific binding/trapping, metabolism and delivery barriers, together with lack of tissue selectivity and relatively low relaxivity (≈ 0.25 s^{-1} mM^{-1}), must be overcome for useful *in vivo* applications.[7,11–14] Some difficulties were, in part, surmounted through the encapsulation or attachment of paramagnetic nitroxide free radicals to biomolecules. For instance, in order to circumvent the problem of

[a] *Dipartimento di Scienze e Tecnologie Biomediche, Università di Milano, Via Fratelli Cervi, 93, I-20090 Segrate (MI), Italy. E-mail: maristella.gussoni@unimi.it; Fax: (+39) 0250330414*
[b] *Istituto per lo Studio delle Macromolecole, Consiglio Nazionale delle Ricerche, Via E. Bassini, 15, I-20133 Milano, Italy. E-mail: lucia.zetta@ismac.cnr.it; Fax: (+39) 0223699212*
[c] *Dipartimento di Chimica Organica e Industriale, Università di Milano, Via Venezian 21, I-20133 Milano, Italy*
[d] *Istituto di Scienze e Tecnologie Molecolari, Consiglio Nazionale delle Ricerche, Via Golgi 19, I-20133 Milano, Italy*

† Glomerular filtration is the renal mechanism of filtering a volume of fluid from the renal glomerular capillaries into the Bowman's capsule. The glomerular filtration rate (GFR, the volume per unit time) is often clinically measured to determine the renal function.

free radical reduction, nitroxides have been encapsulated into liposomes: the system, used for nitroxide *in vivo* delivering, provided an image contrast able to reflect different metabolic conditions.[15] Moreover, albumin–nitroxide complexes, used as contrast agents for MRI, showed proton relaxivities four-fold greater than that of the pure nitroxide,[16] while nitroxyl fatty acid derivatives were able to recognize the same transmembrane transporters as natural fatty acids. Due to their preferential uptake by the non-tumour tissues, they allowed a good delimitation of necrotic tumours.

Recently, polyamido amine dendrimer-linked[17] and methacrylamide copolymer-linked[18] nitroxyl radicals were synthesized and tested as macromolecular contrast agents for MRI of articular cartilages and solid tumours, respectively. In particular, the dendrimer linked nitroxide relaxivities r_1 and r_2 were found to increase linearly with the number of nitroxide groups. This finding was quite surprising, differing from the behavior of the dendrimer-based metal chelates endowed with high molecular weight, whose relaxivities doubled between generations two and six[19] and then reached a plateau at about generation six.[20]

On the other hand, poly(amidoamine)s (PAAs) represent a family of biodegradable and biocompatible polymers containing *tert*-amine and amide groups regularly arranged along the polymer chain.[21–26] They are obtained by Michael-type polyaddition of primary or bis-secondary amines to bis-acrylamides. The first extensive studies on PAA synthesis have been published around 1970[21] and afterwards their chemical properties and biomedical applications have been reviewed in several instances.[21–26] In addition to the amide and *tert*-amine groups present in the main chain, other chemical functions can be introduced as side substituents.

Amphoteric PAAs containing two relatively weak *tert*-amine groups and a single strong carboxyl group per repeating unit can be obtained using 2,2-bis(acrylamido) acetic acid. In particular, a PAA polymer, named ISA23, obtained from 2,2-bis(acrylamido)acetic acid and 2-methylpiperazine (Fig. 1) is predominantly anionic in extracellular fluids, owing to the incomplete ionization of the amino groups and complete ionization of the carboxyl groups at pH 7.4.[25]

Indeed, under a relatively modest lowering of the pH, the polymer passes from a prevailing anionic to a prevailing cationic state. For instance, after intravenous administration, during endocytic internalization, the polymer is transferred from the extracellular fluids at pH 7.4 to the intracellular compartments where the pH is lowered to 6.5 in the endosomes and to around 5.0 in the lysosomes. At low pH, a marked conformational change occurs in ISA23 due to its highly positive charge: in the lysosomal compartment condition the polymer becomes membrane-active, destabilizing the lysosomal membranes, so displaying high haemolytic properties.[26] Moreover, besides being approximately as biocompatible as dextran, ISA23, like any PAA polymer, when injected in animals, is endowed with "stealth" properties, in that it is not recognized by the cells from the rethyculo endothelial system and by a passive process termed the "enhanced permeability and retention (EPR) effect",[26] it selectively concentrates in solid tumor tissues.

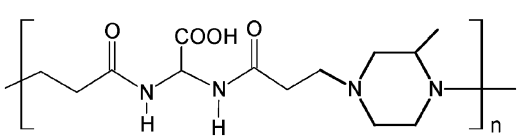

Fig. 1 Structure of ISA23.

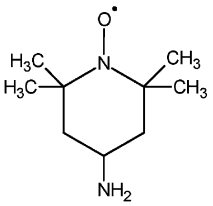

Fig. 2 Structure of Amino-TEMPO.

Therefore PAAs potentially represent, in our opinion, ideal carriers for NMR labeling due to their specific tumor tissue targeting capability. In particular, TEMPO moieties, when covalently bound to PAA amphoteric carriers, might be efficiently transported within body fluids and specifically directed towards tumors.

We thought it would be interesting, therefore, to report here on ISA23 and on two new PAA-TEMPO conjugates, denoted ISA23-TEMPO1 and ISA23-TEMPO2. These last were synthesized by polymerization of 4-amino-2,2,6,6-tetramethylpiperidin-1-oxyl (Amino-TEMPO) as comonomer (Fig. 2). In fact, Amino-TEMPO participates in the polymerization reaction of PAA through its primary amino group, under the conditions normally adopted in the synthesis of PAA. ISA23-TEMPO1 and ISA23-TEMPO2 polymers were endowed with different nitroxide concentration ([NO]): 0.293 and 1.093 mmol g^{-1}, respectively. A thorough NMR structural characterization of ISA23 at different pH values as well as ESR and NMR characterization of ISA23-TEMPO derivatives and the preliminary evaluation of their potential as NMR labels for imaging applications, will be reported. Moreover the enhancement of T_1 polymer relaxivity, namely r_1, attained by increasing the nitroxide concentration, (ISA23-TEMPO1 *vs.* ISA23-TEMPO2), will be also assessed.

2 Results and discussion

2.1 Synthesis of ISA23-TEMPO conjugates

ISA23-TEMPO conjugates, containing 10 and 40% on a molar basis TEMPO residues, were obtained by the direct polyaddition of Amino-TEMPO and 2-methylpiperazine with the lithium salt of 2,2-bis(acrylamido)acetic acid. The synthetic procedure, summarized in Scheme 1, consisted of two polyaddition steps. In the first step, Amino-TEMPO was reacted with a 10 : 1 (or 10 : 4) excess, on a molar basis, lithium 2,2-bis(acrylamido)acetate for few hours until complete reaction, in order to avoid competition by 2-methylpiperazine. It must be observed, in fact, that in primary amines the addition reaction of the first N–H group is relatively fast, whereas that of the second N–H is less favored for both electronic and steric reasons.[27] In the second step, the excess bisacrylamide, that is the 9/10 (or 6/10) of the initial amount, was reacted with an equimolecular amount of

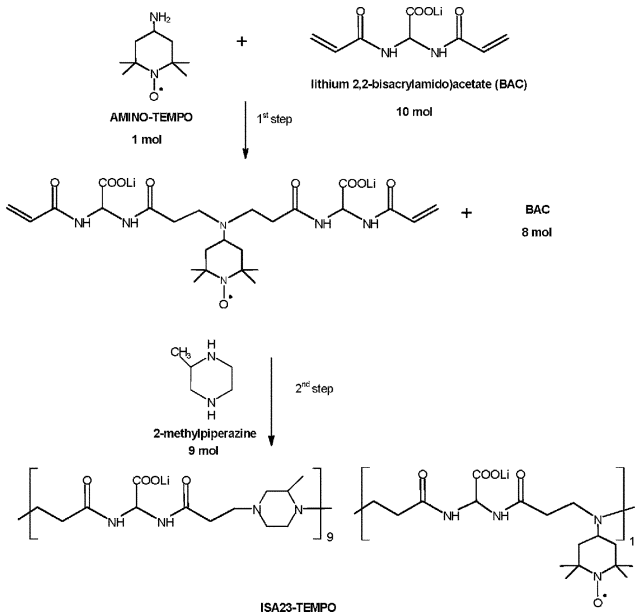

Scheme 1 Synthesis of ISA23-TEMPO conjugate. The indices at the brackets refer to the relative proportion of the different repeating units, but not to the overall polymerization degree.

2-methylpiperazine. The polyaddition reaction was carried out under the conditions normally adopted in PAA synthesis. The final product was recovered by adjusting the pH down to 4.5 and ultrafiltering through a membrane with a nominal molecular weight cut off value of 10 000.

This procedure resulted in some loss of low molecular weight polymer fractions, but gave better products in terms of polydispersity (1.35), that was remarkably low for a polycondensation product. It also brought both ISA23-TEMPO1 and ISA23-TEMPO2 samples to approximately the same molecular weight, albeit at the expenses of a minor yield for the latter.

2.2 NMR structural characterization

^{1}H and ^{13}C NMR spectroscopic investigations on ISA23 polymer were carried out at pH 5 to mimic the conditions that would be encountered upon cellular internalization. Three protonation constants have been reported for ISA23, namely 7.48 and 3.14 for the two amino groups and 2.3 for the carboxylic function. At the pHs encountered upon cellular internalization, the polymer is expected to be in different conditions. At a pH around 5, it is in an almost electrically neutral form as this essentially coincides with its isoelectric point (pH 5.4), where the carboxylate anion is not yet protonated and the second amino group is only partially protonated. On the contrary, at a pH lower than 5, the polymer is totally protonated and hence highly positively charged.

With this in mind, NMR spectroscopy investigations on ISA23 polymer were carried out at both pH 5 and 2, in order to test the change in the average charge when moving towards acidic pH values. Indeed, as previously reported,[26] the change in its average charge results in a marked conformational change from a relative coiled hydrophobic structure to a relaxed hydrophilic open structure that would be assumed within the endosomal and lysosomal cellular compartments.

At both pH 5 and 2, the ^{13}C NMR spectral analysis of ISA23 was performed on the basis of: (i) the intrinsic chemical shifts of different groups, *i.e.* CH_3 and CH_2 covalently bound to carbon nuclei (15–36 ppm), CH_2, CH covalently bound to nitrogen (48–62 ppm), and CONH and COOH (172–176 ppm); (ii) the multiplicity observed in the ^{13}C coupled spectra (CH_3 quartet, CH_2 triplet, CH doublet and CO, COOH singlets) due to $^{1}J_{CH}$, the coupling constant through a single bond; (iii) the value of the $^{1}J_{CH}$, *i.e.* 120–130 Hz for carbons bound to carbons and 140–150 Hz for carbons bound to a nitrogen; (iv) the chemical shifts of *N*,*N*′-diethyl-2-methylpiperazine, assumed as a model; (v) the chemical shift variation as a function of pH and (vi) the heteronuclear multiple bond correlations. Spectral assignments are reported in Table 1.

2.3 NMR at pH 5

The ^{13}C NMR spectrum of ISA23 at pH 5 showed thirteen signals (Fig. 3), that is one signal for each kind of carbon atom. This finding confirmed that, at pH 5, ISA23 is present as a single form LH, protonated only at the more basic amine group of the 2-methylpiperazine moieties.[25]

In the coupled spectrum (Fig. 3 lower) the thirteen signals were: one quartet, due to the CH_3 moiety, seven triplets, two of which due to the two CH_2CO groups and the other five due to the CH_2N groups; two doublets, due to $CHCH_3$ and CHCOO groups and finally three singlets due to the two CON and the COO groups. Of the two doublets, the sharp one at 61.06 ppm belonged to the CHCOO moiety, as deduced from the absence of long range C–H couplings. The five triplets due to the CH_2N groups were tentatively assigned on the basis of the chemical shifts determined for the model compound *N*,*N*′-diethyl-2-methylpiperazine. Starting from the chemical shifts of *N*,*N*′-diethylpiperazine, 52.6 ppm for NCH_2CH_3 and 53.4 ppm for NCH_2CH_2,[28] the additivity contributions (α = 6.0, β = 9.0, γ = 0, δ = −0.5 ppm), due to the presence of an equatorial methyl group in position 2, were added. The additivity contributions of an axial methyl group did not satisfy the experimental PAA chemical shifts, thus the axial methyl could be excluded.

Symbols labelling peaks in the lower spectrum indicate carbon multiplicities, *i.e.* doublet for CH and triplet for CH_2.

A HMBC experiment (Fig. 4) confirmed all the assignments and allowed to attribute the signals at 50.83 and 55.05 ppm to the two kinds of NCH_2CH_2CO, due to their couplings with the adjacent CH_2CO groups. By exclusion, the three signals at 51.75, 52.65 and 58.80, which did not give HMBC correlations, had been assigned to the three NCH_2 carbons of the piperazine ring. All signals belonging to the ring exhibited a line broadening at pH 5, but not at pH 2 (see later), most likely biprotonated (LH_2^{+}) and triprotonated (LH_3^{2+}) forms were present in almost equal amounts: in the former, the two protons were localized on the two amine groups of the 2-methylpiperazine moieties; in the latter, the third proton was localized on the carboxyl group of the 2,2-bis(acrylamido)-acetic moiety.

At pH 2, the ^{13}C chemical shifts (Fig. 5) of the two forms were almost coincident or very close for all carbons except for those belonging to the fragment CH_2CON: indeed, three

Table 1 Chemical shifts (δ) and coupling constants (with multiplicities) of ISA23, at pH 2 and 5, and its nitroxyl radical bearing derivative at pH 5, together with the chemical shifts of the reference model *N*,*N*′-diethylpiperazine and those determined for the model *N*,*N*′-diethyl-2-methylpiperazine by using the additivity contribution of an equatorial methyl in position 2

	ISA23, pH 5 (LH 100%)				ISA23-TEMPO1 conjugate, pH 5 (LH 100%)				ISA23 pH 2 (LH_2^+ and LH_3^{2+} in 1 : 1 ratio)				*N*,*N*′-Diethyl-2-methylpiperazine	*N*,*N*′-Diethylpiperazine[d]
Carbon	δ (ppm)	$^1J_{CH}$/Hz		Area	δ (ppm)	$^1J_{CH}$/Hz		Area	δ (ppm)	$^1J_{CH}$/Hz		Area	δ (ppm)	δ (ppm)
CH_3	16.92	nd	q	0.99	17.01	120.18	q	0.73	16.57	120.01	q	0.99		
CH_2CO[a] (LH_3^{2+})									32.41	130.37	t	0.50		
CH_2CO[a] (LH_3^{2+})									32.52	nd	t	0.50		
CH_2CO (LH_2^+)									32.65	nd	t	1.00		
CH_2CO (LH)	32.96	129.75	t	0.99	32.76	129.01	t	0.90						
CH_2CO[a] (LH)	33.79	129.28	t	0.96	33.64	129.47	t	0.90						
NCH_2CH_2CO	50.83	142.36	t	1.00	50.75	139.19	t	0.92	51.11	147.00	t	0.99	50.1	
CH_2N	51.75	nd	t	0.95	51.81[b]	nd	t	0.72	51.41[b]	146.66	t	0.98	50.9	
CH_2N	52.65	141.44	t	0.95	42.62	145.98	t	0.97	51.66 51.70	149.37	t	0.99	52.4	52.6
NCH_2CH_2CO	55.05	141.35	t	0.92	54.99	nd	t	0.91	55.54	145.31	t	0.96	53.7	
CH_2N	58.50	nd	t	0.92[a]	58.75	nd	t	0.87[a]	56.99 57.04	148.02	t	0.94	62.8	53.4
$CHCH_3$		143.63	d			nd	d		59.36[b]	145.31	d	0.92	62.8	
CHCOOH	61.06	147.83	d	0.94	60.89	147.65	d	1.00	60.90	147.34	d	0.99		
CO (LH_3^{2+})									174.16		s	0.50		
CO (LH_3^{2+})									174.22		s	0.50		
CO (LH_2^+)									174.44		s	1.00		
CO (LH)	174.93		s	0.99	174.83		s	0.95						
CO (LH)	175.52		s	0.94	175.44		s	0.95						
COO^-	175.65		s	1.00	175.70		s	1.00	175.68	6.1[c]	s	0.90		

[a] Average value. [b] Broad signal; [nd] not determined. [c] $^2J_{CH}$. [d] From ref. 28; s: singlet; d: doublet; t: triplet and q: quartet.

signals were observed for the CH_2CO moieties at 32.41, 32.52 and 32.65 ppm with a 1 : 1 : 2 intensity ratio, and for the CO groups at 174.16, 174.22 and 174.44 ppm with the same 1 : 1 : 2 intensity ratio. This finding was in good agreement with the expectation: 50% of the polymer was present as LH_2^+, in which no signal splittings were observed since the double charge on the piperidine ring made the CH_2CON moieties indistinguishable. The other 50% belonged to due to a combination of ring and nitrogen inversion according to Scheme 2.

This line broadening was also observed in the TEMPO derivatives at pH 5, but it disappeared at pH 2 due to the elimination of nitrogen and ring inversion upon exhaustive piperazine protonation.

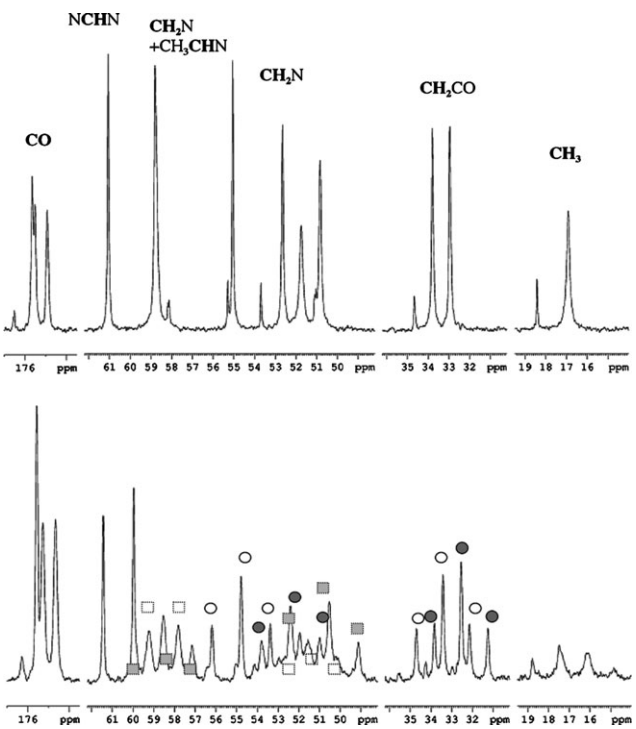

Fig. 3 270 MHz proton decoupled (upper) and coupled (lower) ^{13}C NMR spectra of ISA23 at pH 5.

2.4 NMR at pH 2

While at pH 5 ISA23 was exclusively present as LH form, at pH 2 the LH form was completely absent. Only the biprotonated (LH_2^+) and triprotonated (LH_3^{2+}) forms were present in almost equal amounts: in the former, the two protons were localized on the two amine groups of the 2-methylpiperazine moieties; in the latter, the third proton was localized on the

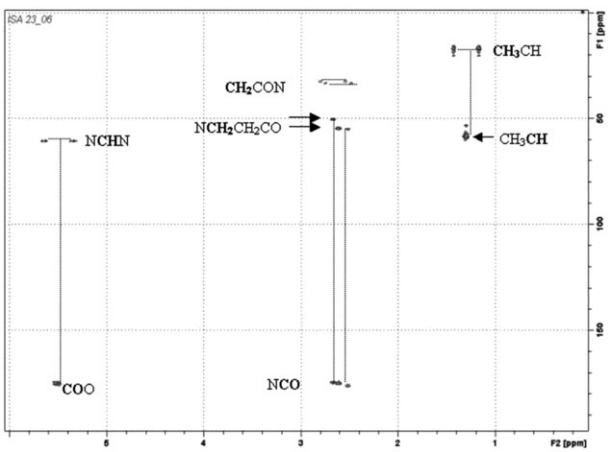

Fig. 4 400 MHz double quantum HMBC (heteronuclear multiple bond correlations) spectrum of ISA23 at pH 5, optimized for a long-range coupling of 5 Hz (100 ms).

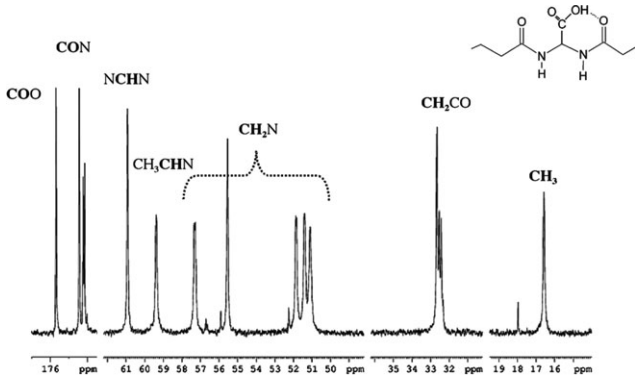

Fig. 5 270 MHz ^{13}C NMR spectrum of ISA23 at pH 2. The inset shows the H-bond possibly present at pH 2 in LH_3^{2+}.

carboxyl group of the 2,2-bis(acrylamido)acetic moiety. At pH 2, the ^{13}C chemical shifts (Fig. 5) of the two forms were almost coincident or very close for all carbons except for those belonging to the fragment CH_2CON: indeed, three signals were observed for the CH_2CO moieties at 32.41, 32.52 and 32.65 ppm with a 1 : 1 : 2 intensity ratio, and for the CO groups at 174.16, 174.22 and 174.44 ppm with the same 1 : 1 : 2 intensity ratio. This finding was in good agreement with the expectation: 50% of the polymer was present as LH_2^+, in which no signal splittings were observed since the double charge on the piperidine ring made the CH_2CON moieties indistinguishable. The other 50% belonged to LH_3^{2+}, in which the CH_2CON moieties were distinguished, due to the possible presence of a H-bond between the carboxylic proton and one of the two amide carbonyls (see inset in Fig. 5). The 1 : 1 ratio of LH_2^+ and LH_3^{2+} forms at pH 2 well fitted the pH titration curves calculated by the basicity constants previously published by some of us.[25] As expected, at pH 2, all signals were sharp, since, in the protonated state, piperazine ring and nitrogen inversions were not possible.

2.5 ISA23-TEMPO1 conjugate at pH 5

The presence of nitroxide units in ISA23-TEMPO1 conjugate did not modify the chemical shift values observed for the PAA at the same pH, as shown in both Fig. 6 and Table 1, this feature suggesting that the introduction of an Amino-TEMPO moiety instead of a piperazine ring did not significantly alter the polymer structure and most likely the polymer properties, while inducing a general area reduction of about 10% in most of the carbon signals. However, an additional selective line

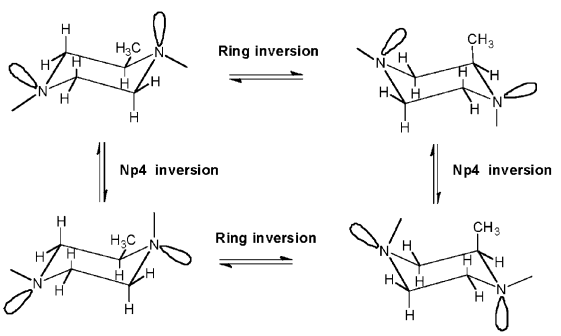

Scheme 2 Ring and nitrogen inversion in 2-methylpiperazine units.

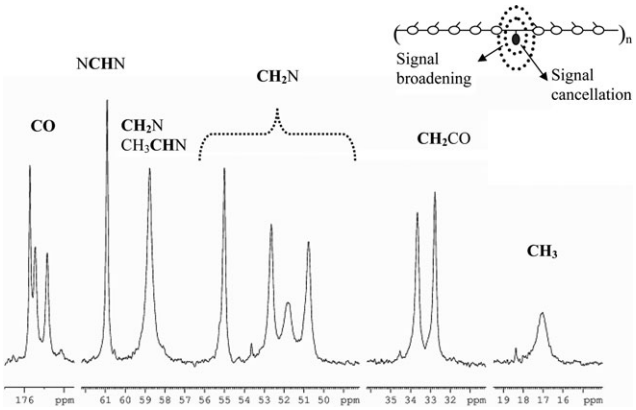

Fig. 6 270 MHz ^{13}C NMR spectrum of ISA23-TEMPO1 at pH 5. The inset shows a sketch of the AMINO-TEMPO effect on the carbon signals. The black filled and the empty symbols represent the AMINO-TEMPO and piperazine moieties, respectively.

broadening, accompanied by a further 20% area reduction, was observed in the three signals of the piperazine ring, corresponding to the CH_3CHN moiety and one of three CH_2N groups. This additional line broadening could only be partially accounted for the piperazine nitrogen and ring inversion observed in ISA23. Most of the broadening effect derived from the presence of the paramagnetic species that increased the relaxation rate of the NMR carbons in the vicinity of the unpaired electrons. As is well known,[29–33] line broadening is proportional to the inverse sixth power of the distance between the label and the reported nucleus, the electron–proton interaction extending over approximately 20–25 Å. Hence, resonances of carbons within about 12 Å of the site of attachment are usually broadened beyond detection, while the line width of resonances within about 16 Å increases significantly, but the corresponding peaks remain observable.

2.6 ESR spectroscopy of ISA23-TEMPO1 conjugate

The experimental spectra of the ISA-TEMPO1 conjugate at pH 2 and 5 are shown in Fig. 7 along with the best-fit computed spectra; the best-fit parameters are reported in Table 2. The best-fit spectra are in excellent agreement with the computed ones. Hence, the lineshape model accounts for all significant contributions to the ESR line shape and width, namely, those due to spin-exchange and molecular rotation. The ESR spectra of the ISA23-TEMPO1 conjugate exhibited the typical three-line pattern due to coupling of the electron spin of the nitroxyl group with the nuclear spin ($I = 1$) of the ^{14}N nucleus. The hyperfine coupling constant a_N, a measure of the strength of the electron spin–nuclear spin coupling, was very close to the literature value of 16.99 G at pH 7.[34] Hence, the Amino-TEMPO electronic structure was not significantly affected by the conjugation into the PAA chain. The slight decrease in a_N at lower pH was ascribable to a more polar environment that shifted spin density from the nitrogen to the oxygen atom of the nitroxyl group. The nuclear spin dependent contributions to the line width B and C (see eqn (2)) provided information about the molecular rotation. The rotational correlation time τ_r estimated from B and C were much longer than that of free Amino-TEMPO (about 0.01 ns at

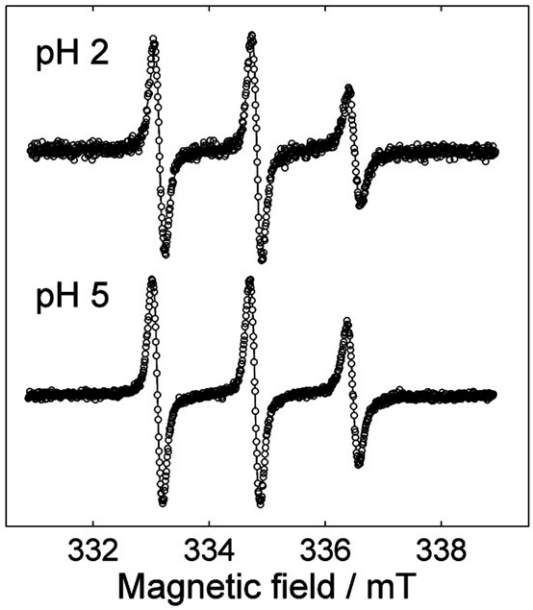

Fig. 7 ESR spectra of ISA23-TEMPO conjugate in physiological solution at pH 2 and 5. Circles: experimental spectrum; solid line: best-fit spectrum.

pH 2), thus confirming that the nitroxyl groups were indeed part of the PAA chain.[35] Besides, the ISA23-TEMPO1 conjugate rotates slower at lower pH. However, rotational frequency was still much larger than the hyperfine coupling constant and the ESR spectrum was purely isotropic, as confirmed by the fact that the lineshape did not deviate from the (complex) Lorentzian shape. The spin exchange interaction W_{xc} was weak ($W_{xc} \ll a_N$) and only slightly affected the ESR spectrum. Spin exchange strongly depended on the inverse distance between the interacting spins, therefore nitroxyl moieties were—on average—closer to each other at pH 5 than at pH 2. Hence, both rotational and spin exchange parameters indicated that the ISA23-TEMPO1 conjugate chain had a more extended conformation at pH 2.

2.7 NMR imaging and relaxivity

As is well known, the contrast in a MR image is the result of a complex interplay of numerous factors including proton density, longitudinal and transverse relaxation times of the imaged tissue. MR image contrast can be further enhanced by using suitable MRI contrast agents. Unlike for X-ray, contrast agents for MRI are not directly visualized in the image. Their

Table 2 Best-fit parameters of the ESR spectra of ISA23-TEMPO conjugate at pH 2 and 5. The *g*-factor, the nitrogen hyperfine coupling constant a_N, the nuclear spin independent contribution to the line width A, and the spin exchange interaction W_{xc} (in magnetic field units) are best-fit parameters. The rotational correlation time τ_r of the conjugate has been estimated from the nuclear spin dependent contributions to the line width B and C

pH	g	a_N/G	A/G	$\tau_r(B)$/ns	$\tau_r(C)$/ns	W_{xc}/G
2	2.0058	16.83	1.16	0.30	0.35	0.25
5	2.0058	16.87	0.95	0.22	0.21	0.55

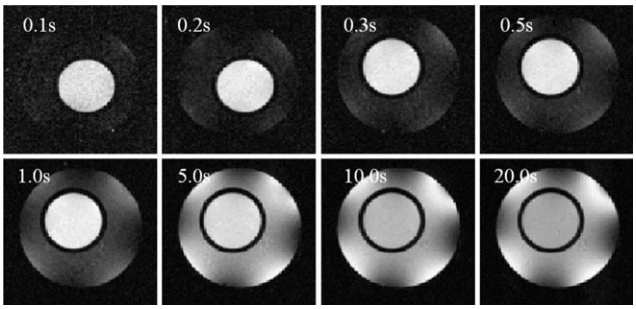

Fig. 8 200 MHz spin-echo images of water (H_2O–D_2O (1 : 1)) and 17.7 mg ISA23-TEMPO conjugate (8 mM concentration of nitroxyl groups) in H_2O–D_2O samples. From the top left to the bottom right: repetition time values are indicated in seconds. Image resolution: $86 \times 86 \times 1000$ μm^3.

effects on the tissue contrast are the results of their ability to reduce the tissue relaxation times.

Fig. 8 reports T_1 weighted images acquired on a ISA23-TEMPO1 sample of 8 mM concentration (internal 5 mm tube) and a control water solution (10 mm external tube). In the range 0.1–5.0 s repetition time, the ISA23-TEMPO1 sample appears hyperintense with respect to the control, the best contrast difference being in the range 0.3–0.5 s repetition time. Therefore, at short repetition times, the addition of ISA23-TEMPO1 polymer to the aqueous solution increases the image proton signal, compared to the reference, owing to the decreased T_1 relaxation in the presence the nitroxyl radical.

Indeed, the T_1 relaxation of saline solution measured at 9.4 T was found to be 3.11 s; at the same field, the T_1 relaxation of a 8 mM nitroxyl groups, was about 1 s, indicating a three times shortening of the T_1 parameter.[36] This feature, combined with the peculiar "stealth" properties, suggested that this polymer can in principle be a potential MR contrast agent to be employed for diagnosis and characterization of solid tumours. In addition, larger numbers of Amino-TEMPO units can be introduced into the polymer, thus decreasing the dose required to achieve the same image contrast enhancement.

As well known, the ability of contrast agents in enhancing proton relaxation rates in the tissue where they distribute, is usually evaluated firstly *in vitro* by the determination of their relaxivity (r_{1p}) which refers to the relaxation enhancement promoted by a given complex at 1 mM concentration.[37]

Thus, the effectiveness of a paramagnetic contrast agent depends not only on its tissue concentration but also on its relaxivity.

Starting from T_1 relaxation measurements, T_1 relaxivity can be calculated from eqn (2) (see Experimental section), that can be re-written as:

$$\Delta(1/T_1) = R[\mathrm{CA}] \qquad (1)$$

where: $\Delta(1/T_1) = 1/T_1 - 1/T_{1CA}$ and $1/T_{1CA}$ and $1/T_1$ are the relaxation rate with and without the polymer contrast agent (CA), that means the relaxation rate of pure saline. Basically, eqn (1) states that relaxation rates, not relaxation times, are additive. The CA relaxivity was calculated from the T_1 data obtained at 9.4 T on the tracer solutions of ISA23-TEMPO1 and ISA23-TEMPO2 by the inversion recovery method, by

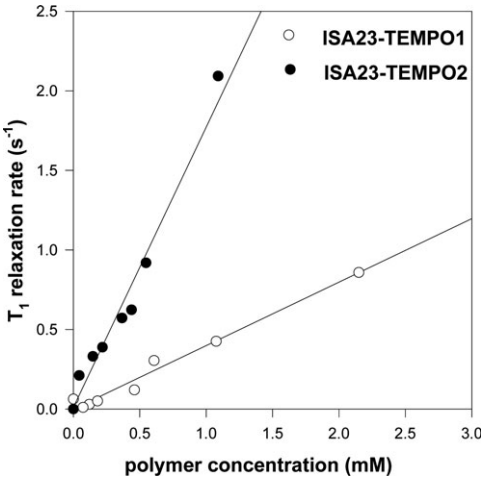

Fig. 9 Relaxation rate values obtained on ISA23-TEMPO1 and ISA23-TEMPO2 plotted as a function of the polymer mM concentration.

subtracting the relaxation rate measured on pure saline, 0.32 s^{-1}, so that the intercept equalled zero.

In Fig. 9 the relaxation rate values obtained on ISA23-TEMPO1 and ISA23-TEMPO2 were plotted as a function of the polymer mM concentration. Increasing the polymer concentration, the relaxation rate increased in a linear fashion for both ISA23-TEMPO1 (○) and ISA23-TEMPO2 (●). The linear regression fitting yielded a relaxivity $R_1 = 0.4\ s^{-1}\ mM^{-1}$ ($r^2 = 0.98$) and $R_1 = 1.8\ s^{-1}\ mM^{-1}$ ($r^2 = 0.99$) for ISA23-TEMPO1 and ISA23-TEMPO2, respectively. By considering that ISA23-TEMPO1 and ISA23-TEMPO2 contained about 4 and about 15 nitroxide units per mmole of polymer, respectively, the intrinsic nitroxide T_1 relaxivity could be calculated as 0.10 and 0.12 $s^{-1}\ mM^{-1}$, respectively. Moreover, nitroxide relaxivity was found to be dependent of the field strength, being almost the same at 4.7 T, while raised to 0.22 $s^{-1}\ mM^{-1}$ when measured at 0.47 T. This value is in agreement with previously reported data on five-membered ring nitroxides: at 8.46 T and 25 °C, several nitroxides showed similar relaxivities of about 0.2 $s^{-1}\ mM^{-1}$.[12] Indeed, Bennett *et al.* reported that the T_1 relaxivity value of ten nitroxides in water was 0.95 ± 0.15 $s^{-1}\ mM^{-1}$ at 2×10^{-4} T (5 °C), falling to 0.30 ± 0.05 $s^{-1}\ mM^{-1}$ at 1.17 T.[37] Also, Lovin *et al.* found the T_1 relaxivities of five nitroxides a factor of 1.7 lower at 2.35 T (23 °C) than at 0.25 T.[38]

Moreover, the relaxivity ratio of the two ISA23 TEMPO derivatives was 4.5. This value was slightly higher than the value expected on the basis of the theoretical nitroxide concentration ratio of 3.7, suggesting that a weak cooperativity exists among the nitroxide moieties of the two polymers, when the number of radical units was increased. On the other hand, this was not surprising, since, as suggested by the NMR and EPR data herein reported, at pH 5, ISA23 should not be completely unfolded. Moreover, the conclusions of the present study are in good agreement with viscosimetric studies, performed by some of us, and self-diffusion data recently published by the Cardiff group, according to which, as expected, close to its isoelectric point, ISA23 has a minimum hydrodynamic volume and a minimum radius, while, far from this, it undergoes a pH driven expansion.[39]

3 Conclusions

From the results reported in this paper, we may draw a series of conclusions.

ISA23 labeled with nitroxyl radicals, denoted ISA23-TEMPO1 and TEMPO2 polymers, were easily prepared with reasonably high reaction yields even after eliminating, by ultrafiltration through a membrane of nominal cut-off 10 000, the lower molecular weight fractions present in the crude reaction products. Apparently, there are no limitations in the percentage of nitroxyl moieties that can be added, at least up to 50% TEMPO containing units. The polymers are always water-soluble at all pH values.

ESR experiments demonstrated that the Amino-TEMPO units were really part of the PAA chain and that the incorporation of a TEMPO unit instead of piperazine does not significantly modify the polymer structure. Besides Amino-TEMPO could be conveniently used as comonomer in PAA synthesis with no detectable alteration of the nitroxyl radical functions. Hence, it can be reasonably expected that the labeling method presented in this paper is of general application for PAAs.

^{13}C NMR spectra exhibited very well conserved chemical shifts for ISA23 and its Amino-TEMPO derivative, confirming the ESR information that the nitroxide function does not affect the polymer conformation and most likely the polymer properties.

Moreover, the ESR parameters, describing molecular rotation and spin exchange, indicated that the ISA23-TEMPO conjugates have a more globular conformation at pH 5 and a more extended one at pH 2, in good agreement with viscosity and diffusion data.[39]

As well, NMR characterization of ISA23 polymer at the two pH values indicated that at pH 5 only the LH form is present, protonated at the more basic amine group of the 2-methylpiperazine moieties, while at pH 2 only the biprotonated (LH_2^+) and triprotonated (LH_3^{2+}) forms are present in 1 : 1 ratio. Therefore, due to the high number of charges distributed along the polymer chain, at pH more acidic than 5, an extended structure of the two polymer is expected. This is in agreement with the findings of Griffiths *et al.* obtained by small angle neutron scattering (SANS) investigations on homopolymeric ISA23.[40]

Preliminary MRI experiments demonstrated that ISA23-TEMPO when dissolved in aqueous solution causes contrast enhancement due to the nitroxyl radical relaxivity. The polymer relaxivity increased linearly from 0.4 to 1.8 $s^{-1}\ mM^{-1}$ with the increase of nitroxyl number from 1 to 3.7 in the repetition units of ISA23-TEMPO1 and ISA23-TEMPO2, respectively. It is worth noting that when comparing the relaxivity ratio, 4.4, of the two polymers with their nitroxyl concentration ratio, 3.7, a weak cooperative interaction could be supposed among the nitroxide moieties, most likely due to a not too large mean distance among them.

As a final conclusion, ISA23-TEMPO synthesized polymers have a definite potential as NMR imaging contrast agents.

Even if, as is well known, nitroxide relaxivity is not too high, the stealth properties, reported elsewhere by some of us,[26] do assure that high concentrations of labeled polymer can be introduced in solid tumours. Moreover, lack of an effective lymphatic system shall lead to retention of this material in the tumour for a sufficient time to be detected.

4 Experimental

4.1 Materials

4-Amino-2,2,6,6-tetramethylpiperidin-1-oxyl (Amino-TEMPO) (>98.0%) and lithium hydroxide monohydrate (>98.0%) were purchased from Fluka and used without further purification. 2-Methylpiperazine, also purchased from Fluka, was recrystallized from *n*-heptane and its purity determined titrimetrically just before use. 2,2-Bis(acrylamido)acetic acid was synthesized according to a procedure already reported[41] and its purity determined titrimetrically just before use.

4.2 Synthesis of ISA23-TEMPO1 and ISA23-TEMPO2

A mixture of 2,2-bis(acrylamido)acetic acid (1.00 g, 5.07 mmol), lithium hydroxide monohydrate (0.213 g, 5.07 mmol) and water (1.6 ml) were stirred until a clear solution was obtained. Amino-TEMPO (0.087 g, 0.50 mmol) was then added with stirring and the resultant mixture maintained at room temperature under a nitrogen atmosphere for 20 h. After this time, 2-methylpiperazine (0.457 g, 4.563 mmol) was added and the reaction mixture maintained two days at room temperature in the dark under nitrogen with occasional stirring. The reaction mixture was then diluted to 200 ml with water and the pH adjusted to 5.0 with small amounts of 37% hydrochloric acid. The product was finally purified by ultrafiltering through a membrane with a nominal cut-off of 10 000, and recovering by freeze drying the retained portion. The reaction yield was 0.95 g (62%). The lower molecular weight fraction passed through the membrane was not recovered.

The same procedure as in the previous case was followed, starting from 0.348 g (2.028 mmol) Amino-TEMPO, 0.305 g (0.304 mmol) 2-methylpiperazine and the same quantities of the other reagents. The product was isolated in the same way. The reaction yield was 0.92 g (55.7%). Also in this case the lower molecular weight fraction passed through the membrane was not recovered. ISA23-TEMPO1 and ISA23-TEMPO2 had about the same molecular weight (M_n = 10 000, M_w = 13 500) and polydispersity index (1.35).

4.3 Size exclusion chromatography

Size exclusion chromatograms were obtained making use of TSK-gel G5000 PW, TSK-gel G4000 PW and TSK-gel G3000 PW columns produced by TosoHaas. The three columns were connected in series. The mobile phase was 0.1 molar Tris buffer pH 8.10 containing 0.2 mol l^{-1} sodium chloride; the flow rate was 1 ml min^{-1} (Waters model HPLC pump 515); the UV detector was a Waters model 486, operating at 230 nm; the refractive detector was a Waters model 2410. The samples for analysis were prepared in the same Tris buffer used as mobile phase (10 mg polymer in 1 ml buffer).

4.4 NMR spectroscopy

All NMR experiments were performed at 25 °C on Bruker AM-270 and Avance 400 spectrometers (Bruker, Karlsruhe, Germany), operating at 67.9 and 100 MHz, respectively, for ^{13}C. The monodimensional ^{13}C NMR spectra were obtained with and without proton decoupling, using standard pulse sequences. The ^{13}C spectral parameters were as follows: spectral width, 20 kHz; recycle delay, 15 s; around 5000 transients, recorded by using 64 K data points, with a spectral resolution of 0.6 and 0.4 Hz (at 270 and 400 MHz, respectively), and a line-broadening factor of 3 Hz before Fourier transformation. The double quantum HMBC (heteronuclear multiple bond correlations) experiment,[42] acquired at 400 MHz, was optimized for a long-range coupling of 5 Hz (100 ms). Spectral parameters were as follows: TD = 2 K and 256 increments, ^{1}H $\pi/2$ pulse = 16.4 μs (5 dB attenuation), ^{13}C $\pi/2$ pulse = 12.3 μs (−3.5 dB attenuation), ^{1}H SW = 6 ppm, ^{13}C SW = 50 ppm, number of scans = 64. Water was presaturated. Proton decoupling was not applied during acquisition.

4.5 ESR spectroscopy

Electron spin resonance experiments were performed on a Bruker ElexSys E500 spectrometer equipped with a Bruker E036 NMR teslameter and a Hewlett-Packard 5340A frequency meter. ISA23-TEMPO1 conjugate was dissolved in physiological solution at such concentration that the concentration of nitroxyl groups is 1 mM. The pH was adjusted to 2 or 5 with hydrochloric acid just prior to the experiments. The samples were accurately purged with nitrogen and then sealed in glass capillaries. Typical experimental conditions were: microwave frequency 9.4 GHz, microwave power 0.1 mW, field amplitude modulation 0.2 G. Instrumental parameters are such as not to affect the width and shape of the three lines of the nitroxide spectrum. ESR spectra were fitted to a spectral model which accounts for second order hyperfine effects on the line position and for contributions to the line width due to molecular rotation.[14] The latter makes the line width R dependent on the nitrogen nuclear spin quantum number m:

$$R(m) = A + Bm + Cm^2 \quad (2)$$

The shape of the ESR line departs from pure Lorentzian absorption shape because of the coupling of microwaves to the aqueous solvent which causes admixture with Lorentzian dispersion shape.[43] A similar effect is brought about by the interaction between different nitroxyl groups, *i.e.*, spin exchange interaction, which also affects both line position and width.[44,45]

4.6 NMR imaging

MRI experiments were carried out on a 4.7 Tesla Bruker AM WB superconducting magnet (Bruker, Karlsruhe, Germany) with a 9 cm diameter vertical bore, equipped with a probehead tuned at the ^{1}H resonance frequency (200.13 MHz), a 15 mm insert, accepting 10 mm NMR tubes. Orthogonal field gradient coils, built into the micro-imaging probe head, were capable of achieving gradients up to 150 G cm^{-1}, with trigger pulses for switching the gradients of 5 μs. Since in this configuration the instrument was not provided with field

frequency stabilization (lock channel), at the beginning of the experiment the field frequency was set on the water resonance frequency. MRI experiments were carried out employing a phase/frequency encoding 2D spin-echo pulse sequence, standardly supplied by Bruker. Acquisition parameters were: spectral width of 33 kHz; variable relaxation time ($D1$) of 0.1, 0.2, 0.3, 0.5, 1.0, 5.0, 10.0, 20.0 s, with consequent variable recycle times (T_R = 6.2 ms + $D1$). Transversal images were characterized by: field of view (FOV) = 11 mm, 256 × 256 matrix, SW = 33 kHz, NE = 10, slice thickness: 1 mm, planar resolution: 86 × 86 μm^2. MRI experiments were carried out on a phantom consisting of a 10 mm NMR tube filled with D_2O–H_2O (1 : 1), containing a coaxial 5 mm NMR tube filled with 600 μl D_2O–H_2O (1 : 1) plus 17.7 mg of ISA23-TEMPO conjugate, corresponding to [NO] = 8 mM. All images were acquired under the same conditions and displayed at the same grey scale levels to be able to compare them. Image reconstructions and elaborations were performed on a O2 Workstation (Silicon Graphics, Mountain View, California) by using the Paravision software package (Version 2.6) standardly provided by Bruker.

4.7 T_1 measurements and NMR relaxivity

Test samples were prepared for T_1 spectroscopic measurements by diluting known amounts of ISA23-TEMPO1 and ISA23-TEMPO2 in saline solution (NaCl 9 g l^{-1}). For each polymer, nine model solutions were obtained with [NO] ranging from 0.3 to 32 mM, at pH 5. Each solution was put in a test tube, coaxially introduced in a 5 mm NMR tube, filled with deuterated toluene (Toluene d_8, Merck) to gain the lock signal. Each sample was deoxygenated, by bubbling nitrogen through the solution for about 10 min immediately prior to the experiment. Longitudinal relaxation (T_1) measurements were performed at 400 MHz on a 7 T Bruker Avance spectrometer (Bruker, Karlsruhe, Germany) by using a standard inversion–recovery (IR) sequence. The IR time (t) was varied between 10 μs and 20 s (number of experiments NE = 30). The repetition time, TR, was 20 s, *i.e.* five times longer than the T_1 value of pure saline (3.11 s, 0.0259 SD). All measurements were performed at 25 °C. The integrals of the water peaks in the ^{1}H spectra *vs.* the corresponding time t, were used to calculate the T_1 values by means of the supplied XWIN NMR Bruker software, fitting the data to a monoexponential function. T_1 relaxivity was then calculated by fitting the T_1 data, obtained at different nitroxide concentrations, to the following equation:

$$1/T_{1obs} = 1/T_{1w} + R_{T1}[NO] \quad (3)$$

where T_{1obs} = T_1 measured value; T_{1w} = T_1 relaxation in the absence of NO-polymer, *i.e.* T_1 of the pure saline; [NO]: nitroxide concentration of the sample solution; R_{T1}: constant defining the relaxivity of the polymer. Experimental data were fitted by the Marquardt–Levenberg algorithm implemented by the Sigma-Plot software (Jandel).

Acknowledgements

The authors are grateful to Giulio Zannoni for helpful technical assistance.

References

1 K. Matsuda and H. Iwamura, *Curr. Opin. Solid State Mater. Sci.*, 1997, **2**, 446–450.
2 E. G. Rozantsev, *Free Nitroxyl Radicals*, Plenum Press, New York–London, 1970.
3 J. B. Mitchell and A. Samanuni, *Biochemistry*, 1990, **29**, 2802–2807.
4 T. Gnewuch and G. Sosnovsky, *Chem. Rev.*, 1986, **86**, 203–238.
5 T. K. Kovacs and A. D. Dean Sherry, *J. Am. Chem. Soc.*, 2002, **124**, 3514–3515.
6 H. M. McConnell, in *Molecular Motion in Biological Membranes*, ed. L. J. Berliner, Academic Press, New York, 1976, pp. 525–560.
7 R. C. Brasch, D. A. London, G. E. Wesbey, T. N. Tozer, D. E. Nitecki, R. D. Williams, J. Doemeny, L. D. Tuck and D. P. Lallemand, *Radiology*, 1983, **147**, 773–779.
8 R. L. Ehman, G. E. Wesbey, K. L. Moon, R. D. Williams, M. T. McNamara, W. R. Couet, T. N. Tozer and R. C. Brasch, *Magn. Reson. Imaging*, 1985, **3**, 89–97.
9 J. F. Glockner, H.-C. Chan and H. M. Swartz, *Magn. Reson. Med.*, 1991, **20**, 123–133.
10 A. M. F. Benial, K. Ichikawa, R. Murugesan, K.-i. Yamada and H. Utsumi, *J. Magn. Reson.*, 2006, **182**, 273–282.
11 J. F. W. Keana, S. Pou and G. M. Rosen, *Magn. Reson. Med.*, 1987, **3**, 83–88.
12 P. Caravan, J. J. Ellison, T. J. McMurry and R. B. Lauffer, *Chem. Rev.*, 1999, **99**, 2293–2352.
13 A. Iannone, A. Tomasi, V. Vannini and H. M. Swartz, *Biochim. Biophys. Acta*, 1990, **1034**, 290–293.
14 H. M. Swartz, M. Sentjurc and P. D. Morse, *Biochim. Biophys. Acta*, 1986, **888**, 82–89.
15 J. F. W. Keana, *US Pat.*, 4863717, 1989.
16 H.-C. Chan, K. Sun, R. L. Magin and H. M. Swartz, *Magn. Reson. Med.*, 1988, **8**, 160–170.
17 C. S. Winalski, S. Shortkroff, R. V. Mulkern, E. Schneider and G. M. Rosen, *Magn. Reson. Med.*, 2002, **48**, 965–972.
18 Y. Huang, A. Nan, G. M. Rosen, C. S. Winalski, E. Schneider, P. Tsai and H. Ghanderhari, *Macromol. Biosci.*, 2003, **3**, 647–652.
19 E. C. Wiener, M. W. Brechbiel, H. Brothers, R. L. Magin, O. A. Gansow, D. A. Tomalia and P. C. Lauterbur, *Magn. Reson. Med.*, 1994, **31**, 1–8.
20 L. H. Bryant, Jr, M. W. Brechbiel, C. Wu, J. W. Bulte, V. Herynek and J. A. Frank, *Magn. Reson. Imaging*, 1999, **9**, 348–352.
21 F. Danusso and P. Ferruti, *Polymer*, 1970, **11**, 88–113.
22 P. Ferruti, in *Polymeric Materials Encyclopedia*, ed. J. C. Salamone, CRC Press, Boca Raton, FL, 1996, vol. 5, p. 3334.
23 P. Ferruti, M. A. Marchisio and R. Barbucci, *Polymer*, 1985, **26**, 1336–1348.
24 P. Ferruti, M. A. Marchisio and R. Duncan, *Macromol. Rapid Commun.*, 2002, **23**, 332–355.
25 P. Ferruti, S. Manzoni, S. Richardson, R. Duncan, N. G. Patrick, R. Mendichi and M. Casolaro, *Macromolecules*, 2000, **33**, 7793–7797.
26 S. Richardson, P. Ferruti and R. Duncan, *J. Drug Targeting*, 1999, **6**, 391–404.
27 P. Ferruti, S. Knobloch, E. Ranucci, R. Duncan and E. Gianasi, *Macromol. Chem. Phys.*, 1998, **199**, 2565–2575.
28 M. K. Denk, M. J. Krause, D. F. Niyogi and N. K. Gill, *Tetrahedron*, 2003, **59**, 7565–7570.
29 G. M. Clore and C. D. Schwieters, *Curr. Opin. Struct. Biol.*, 2002, **12**, 146–153.
30 V. Gaponenko, J. W. Howarth, L. Columbus, G. Gasmi-Seabrook, J. Yuan, W. L. Hubbell and P. R. Rosevear, *Protein Sci.*, 2000, **9**, 302–309.
31 G. Cornilescu and A. Bax, *J. Am. Chem. Soc.*, 2000, **122**, 10143–10154.
32 A. Ramos and G. Varani, *J. Am. Chem. Soc.*, 1998, **120**, 10992–10993.
33 C. H. M. Papavoine, R. N. H. Konings, C. W. Hilbers and F. J. M. van de Ven, *Biochemistry*, 1994, **33**, 12990–12997.
34 B. R. Knauer and J. J. Napier, *J. Am. Chem. Soc.*, 1976, **98**, 4395–4400.
35 N. M. Atherton, in *Principles of Electron Spin Resonance*, ed. E. Horwood, Chichester UK, 1993.
36 M. Gussoni, unpublished results.

37 H. F. Bennett, R. D. Brown, S. H. Koenig and H. M. Swartz, *Magn. Reson. Med.*, 1987, **4**, 93–111.
38 J. D. Lovin, G. E. Wesbey, B. L. Engelstad, G. Sosnovsky, M. Mosely, D. L. Tuck and R. C. Brasch, *Magn. Reson. Imaging*, 1985, **3**, 73–81.
39 Z. Khayat, P. C. Griffiths, I. Grillo, R. K. Heenan, S. M. King and R. Duncan, *Int. J. Pharm.*, 2006, **317**, 175–86.
40 P. Griffiths, Z. Khayat, S. Tse, R. Heenan, S. King and R. Duncan, *Biomacromolecules*, 2007, **8**, 1004–1012.
41 P. Ferruti, E. Ranucci, F. Trotta, E. Gianasi, G. E. Evagorou, M. Wasil, G. Wilson and R. Duncan, *Macromol. Chem. Phys.*, 1999, **200**, 1644–1654.
42 A. Bax and M. F. Summers, *J. Am. Chem. Soc.*, 1986, **108**, 2093–2094.
43 M. Sueki, G. A. Rinard, S. S. Eaton and G. R. Eaton, *J. Magn. Reson., Ser. A*, 1996, **118**, 173–188.
44 B. L. Bales and M. Peric, *J. Phys. Chem. B*, 1997, **101**, 8707–8716.
45 M. Peric and B. L. Bales, *J. Magn. Reson.*, 2004, **169**, 27–29.

